

# Catalytic Microreactors for Portable Power Generation

Bearbeitet von  
Symeon Karagiannidis

1. Auflage 2011. Buch. xvi, 112 S. Hardcover

ISBN 978 3 642 17667 8

Format (B x L): 15,5 x 23,5 cm

Gewicht: 364 g

[Weitere Fachgebiete > Technik > Energietechnik, Elektrotechnik > Energieumwandlung, Energiespeicherung](#)

Zu [Inhaltsverzeichnis](#)

schnell und portofrei erhältlich bei

  
DIE FACHBUCHHANDLUNG

Die Online-Fachbuchhandlung [beck-shop.de](http://beck-shop.de) ist spezialisiert auf Fachbücher, insbesondere Recht, Steuern und Wirtschaft. Im Sortiment finden Sie alle Medien (Bücher, Zeitschriften, CDs, eBooks, etc.) aller Verlage. Ergänzt wird das Programm durch Services wie Neuerscheinungsdienst oder Zusammenstellungen von Büchern zu Sonderpreisen. Der Shop führt mehr als 8 Millionen Produkte.

## Chapter 2

# Experimental Setup

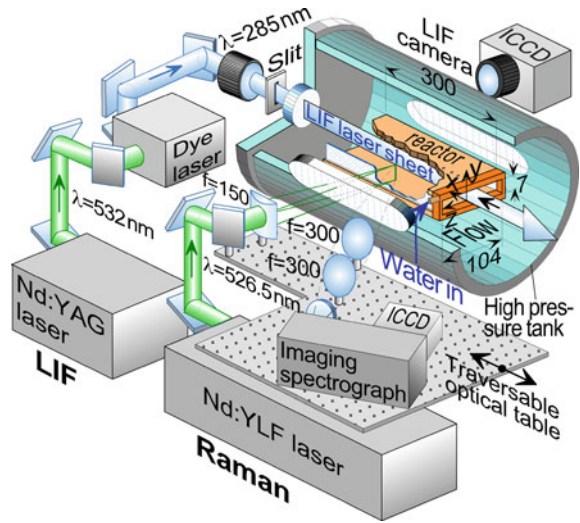
### 2.1 High-Pressure, Optically Accessible, Catalytic Channel-Flow Reactor

The test rig employed in this study consisted of a high-pressure cylindrical steel vessel with a length of 1.8 m and an internal diameter of 0.28 m. Visual inspection and accessibility of the reactor assembly was achieved via a 50 mm diameter quartz window at the rear flange of the vessel and two 350 mm long and 50 mm high quartz windows at the vessel sides. The test setup (Fig. 2.1) consisted of a channel-flow catalytic reactor, which was mounted inside the high-pressure cylindrical vessel. The reactor comprised two horizontal Si[SiC] plates with a length ( $x$ ) of 300 mm, width ( $z$ ) of 104 mm and thickness of 9 mm; the plates were positioned 7 mm apart ( $y$ ). The other two sides of the reactor were formed by two 3-mm-thick vertical quartz windows.

The inner surfaces of the Si[SiC] plates were coated via plasma vapor deposition with a 1.5  $\mu\text{m}$  thick  $\text{Al}_2\text{O}_3$  non-porous layer, followed by a 2.2  $\mu\text{m}$  thick platinum layer. BET and CO-chemisorption measurements verified the absence of porous structures in the catalyst layer [1]. The surface temperatures along the  $x$ - $y$  symmetry plane were monitored with S-type thermocouples (12 for each plate), which were embedded 0.9 mm beneath the catalyst layer. In order to facilitate the ensuing catalytic reactivity studies, a kinetically-controlled fuel conversion away from the mass-transport-limit was necessary. To avoid transport limitations originating from the high catalytic reactivity of propane over platinum, a coupled cooling/heating arrangement was adopted to control the surface temperatures: in a fashion similar to earlier hydrogen catalytic combustion studies [2], the reactor entry section was water-cooled to maintain a low catalytic reactivity while the rear of the reactor ( $x > 100$  mm) was heated by two resistive heaters placed above the ceramic plates.



**Fig. 2.2** Test rig and Raman/LIF setup



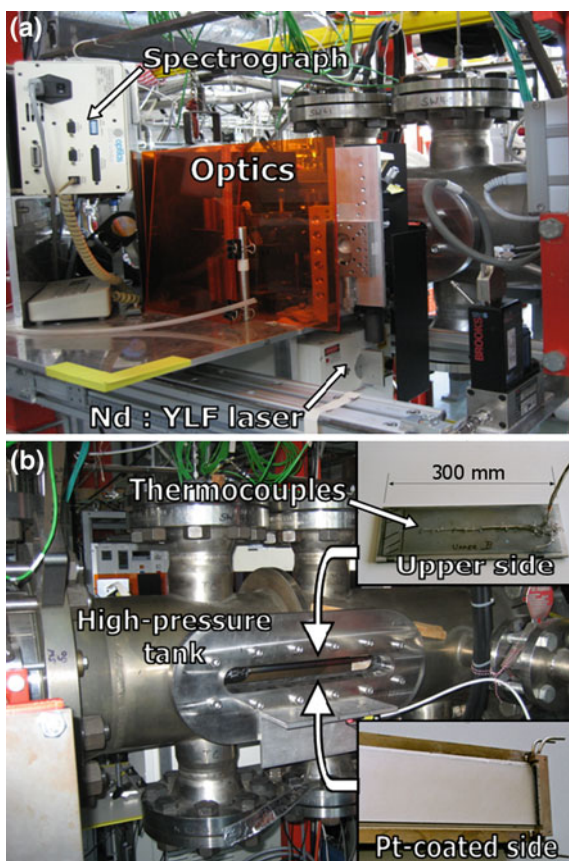
## 2.2 Laser Diagnostics: Raman Spectroscopy and OH-LIF

The LIF/Raman set-up is shown in Fig. 2.2. The particularly low volumetric content of fuel in lean propane/air combustion necessitated the use of a dedicated high power laser for the Raman measurements. The 526.5 nm radiation of a high repetition rate, frequency-doubled Nd:YLF pulsed laser (Quantronix Darwin Duo), operated at 1.5 to 2 kHz, with a pulse duration and energy of 130 ns and 37 to 43 mJ, respectively, provided the light source for the Raman measurements. Given the laminar and steady operating conditions, the signal of 20,000–40,000 pulses was integrated on the detector chip when acquiring an image. Six of these images were subsequently averaged, such that up to 9 kJ of laser light was used for a single Raman spectrum. The signal-to-noise ratio increased by a factor of 20 compared to the previous methane/air Raman arrangement [3, 4]; moreover, the danger of dielectric gas breakdown was eliminated due to the resulting lower intensities at the focal line. The 526.5 nm beam was focused through the vessel and reactor side-windows into a vertical line ( $\sim 0.3$  mm thick) by an  $f = 150$  mm cylindrical lens. The focal line spanned the 7 mm channel separation and was offset laterally ( $z = 15$  mm) to increase the collection angle and minimize thermal beam steering [4]. Two  $f = 300$  mm lenses collected the scattered light at a  $50^\circ$  angle with respect to the incident optical path and focused it to the entrance slit of a 25 cm imaging spectrograph (Chromex-250i) equipped with an intensified CCD camera (Princeton Instruments PI-MAX1024GIII). The 1024- and 256-pixel-long CCD dimensions corresponded to wavelength and transverse distance, respectively. The effective Raman cross sections, which included transmission efficiencies, were evaluated by recording the signals of pure propane, air, and completely burnt gases of known composition. Raman data for the major combustion species  $C_3H_8$ ,  $H_2O$ ,  $N_2$ ,  $O_2$  and  $CO_2$  were acquired at different positions by traversing axially a table supporting the

sending and collecting optics and also the Nd:YLF laser (Fig. 2.2). The 250-pixel-long 7 mm channel height was binned to 63 pixels.

For the OH-LIF, the 532 nm radiation of a frequency-doubled Nd:YAG laser (Quantel TDL90 NBP2UVT3) pumped a tunable dye laser (Quantel TDL90); its frequency-doubled radiation (285 nm) had a pulse energy of 0.5 mJ, low enough to avoid saturation of the  $A(v = 1) \leftarrow X(v' = 0)$  transition. The 285 nm beam was transformed into a laser sheet by a cylindrical lens telescope and a 1 mm slit mask, which propagated counterflow, along the  $x$ - $y$  symmetry plane (Fig. 2.2). The fluorescence of both (1-1) and (0-0) transitions at 308 and 314 nm, respectively, was collected at  $90^\circ$  (through the reactor and vessel side-windows) with an intensified CCD camera (LaVision Imager Compact HiRes IRO,  $1,392 \times 1,024$  pixels binned to  $696 \times 512$ ). A  $120 \times 7$  mm<sup>2</sup> section of the combustor was imaged on a  $600 \times 34$  pixel CCD-area. The camera was traversed axially to map the 300 mm reactor extent; at each measuring location 400 images were averaged. A picture of the actual test rig mounted with optics and Raman set-up is provided in Fig. 2.3, along with pictures of the platinum-coated plates, complete with the embedded thermocouples.

**Fig. 2.3** Optics, spectrograph and Nd:YLF laser mounted on the test rig (a), and side view of the high-pressure test rig (b), along with pictures of the platinum-coated and thermocouple-fitted sides of a reactor plate



## 2.3 Subscale Catalytic Honeycomb Combustor

The honeycomb catalytic burner tested in this work was a subscale version of the actual catalytic combustor proposed for the micro-gas-turbine-based power unit, and was embedded inside the high-pressure vessel (see Fig. 2.4). It comprised a 35 mm inner-diameter, 75 mm long ( $L$ ) and 1.5 mm thick steel tube, wherein alternating flat and corrugated FeCr-alloy foils (with thickness  $\delta = 50 \mu\text{m}$ ) were rolled up forming a honeycomb structure with a channel density of 400 cpsi.

Visual inspection of the subscale unit revealed an overall good cross-section uniformity for the catalytic channels (see Fig. 2.4). The unit tested in this study differed from the proposed mesoscale catalytic combustor only in its inner diameter (all other geometric parameters were kept constant), with the former unit having a radial dimension  $\sim 42\%$  smaller than the latter. With the number of catalyst-coated channels being proportional to the honeycomb cross sectional area, the power output of the subscale unit was reduced nearly threefold compared to the mesoscale unit; heat losses from the outer combustor surface were accordingly impacted due to the reduced surface area of the subscale combustor.

The cross section of each channel was triangular with rounded corners and the equivalent hydraulic radius was  $r_h = 0.507 \text{ mm}$ . The FeCr-alloy foils were coated with a porous 5%-wt Pt/Al<sub>2</sub>O<sub>3</sub> washcoat of  $\sim 15 \mu\text{m}$  thickness. Details on the

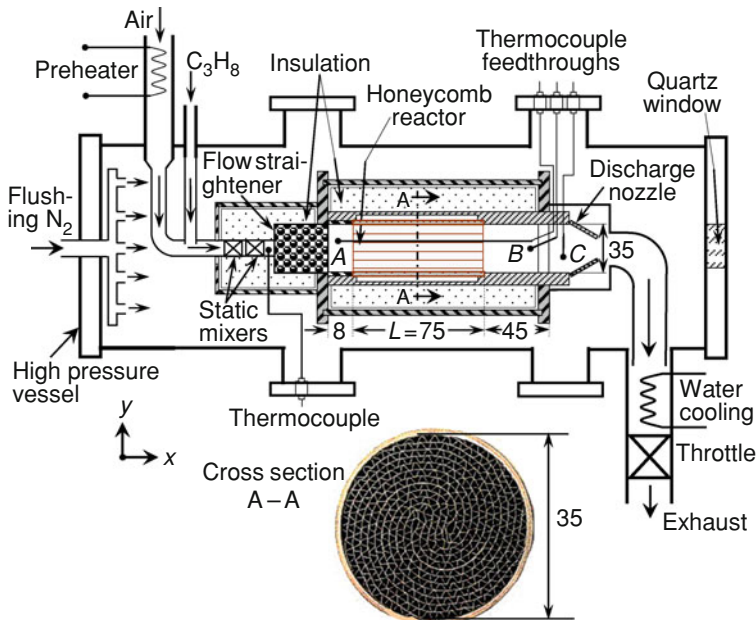
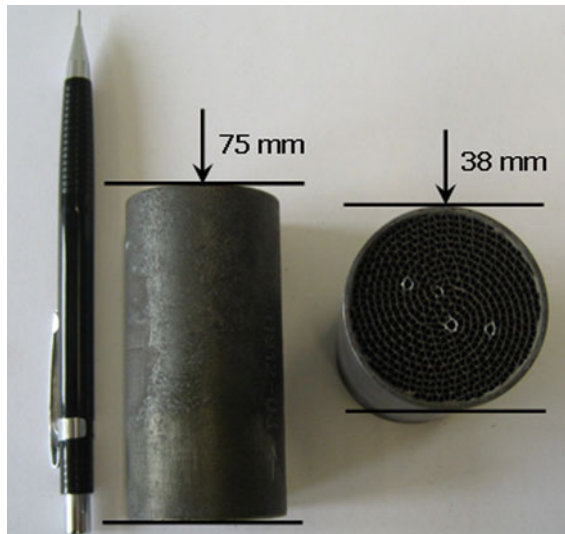


**Fig. 2.4** High-pressure test rig fitted with the honeycomb catalytic combustor. Points  $A$ ,  $B$  and  $C$  denote the thermocouple positions. Cross-section  $A-A$  presents a top-down view of the subscale catalytic combustor. All distances are in mm

catalytic washcoat preparation can be found elsewhere [5]. BET and  $H_2$ -chemisorption measurements of the fresh Pt-coated foils determined the active-to-geometrical surface ratio of the catalytic washcoat; this value was found to be equal to  $B = 15$  and was later used as input in the computational model developed to simulate the entire honeycomb monolith structure.

High pressure bottles supplied technical grade (99.5% purity) propane, and dry air was supplied by a compressor. Two Brooks mass-flow meters regulated the corresponding flows. The air flow was preheated by a 3 kW resistive heater and then mixed with room temperature propane in two sequential static mixers. A follow-up 40 mm long packing of 2 mm diameter ceramic spheres straightened the flow. The reactor was mounted inside an insulated (using a 30-mm-thick fiber ceramic material) cylindrical steel frame and was affixed 8 mm downstream of the flow straightener (Fig. 2.4). Only the first and last 2 mm of the reactor contacted the steel frame, while in the remaining length a 1-mm-thick annular air-cushion was available. In order to regulate the temperature inside the high pressure vessel, air flowed in the free volume between the reactor and the vessel. The inlet and outlet reactor temperatures were monitored with three 50- $\mu\text{m}$  thick K-type (Ni/Cr–Ni/Al) sheathed thermocouples (designated A through C in Fig. 2.4). The thermocouple beads were positioned at  $x = -15, 95$  and  $125$  mm, with  $x = 0$  denoting the beginning of the combustor monolith. The absolute accuracy of the gas temperature measurements was  $\sim 10$  K for the hot outlet and  $\sim 6$  K for the inlet. A picture of the honeycomb catalytic combustor tested is provided in Fig. 2.5.

**Fig. 2.5** Subscale, catalytic, honeycomb combustor



## References

1. Reinke M, Mantzaras J, Bombach R, Schenker S, Inauen A (2005) Gas-phase chemistry in catalytic combustion of methane/air mixtures over platinum at pressures of 1 bar to 16 bar. *Combust Flame* 141:448–468
2. Appel C, Mantzaras J, Schaeren R, Bombach R, Inauen A, Kaeppli B, Hemmerling B, Stampanoni A (2002) An experimental and numerical investigation of homogeneous ignition in catalytically stabilized combustion of hydrogen/air mixtures over platinum. *Combust Flame* 128:340–368
3. Reinke M, Mantzaras J, Schaeren R, Bombach R, Inauen A, Schenker S (2004) High-pressure catalytic combustion of methane over platinum: in situ experiments and detailed numerical predictions. *Combust Flame* 136:217–240
4. Reinke M, Mantzaras J, Schaeren R, Bombach R, Inauen A, Schenker S (2005) Homogeneous ignition of CH<sub>4</sub>/air and H<sub>2</sub>O- and CO<sub>2</sub>-diluted CH<sub>4</sub>/O<sub>2</sub> mixtures over platinum; an experimental and numerical investigation at pressures up to 16 bar. *Proc Combust Inst* 30:2519–2527
5. Eriksson S, Wolf M, Schneider A, Mantzaras J, Raimondi F, Boutonnet M, Järas S (2006) Fuel-rich catalytic combustion of methane in zero emissions power generation processes. *Catal Today* 117:447–453